Available online at www.sciencedirect.com
ScienceDirect
Trans. Nonferrous Met. Soc. China 35(2025) 3949−3960
Transactions of Nonferrous Metals Society of China
www.tnmsc.cn

Enhancement of rust leaching by frame blades and its mechanisms

Lei ZHOU, Qiu-yue ZHAO, Guo-zhi LV, Zhi-he DOU, Ting-an ZHANG

Key Laboratory of Ecological Metallurgy of Multi-metal Intergrown Ores of Ministry of Education, Special Metallurgy and Process Engineering Institute, School of Metallurgy, Northeastern University, Shenyang 110819, China

Received 4 March 2024; accepted 22 November 2024

Abstract: Frame blades were used to replace traditional propeller blades to enhance the leaching step efficiency of Becher process. A combined approach of leaching, electrochemical experiments, and numerical simulations was employed. Results demonstrate a significant improvement in leaching efficiency using frame blades compared to propellers, reducing reaction time from 15 to 10 h. Even at a stirring speed of 300 r/min, frame blades perform better than propellers at 500 r/min. Kinetics analysis indicates that the leaching process is controlled by surface chemical reactions. CFD−PBM simulations reveal that frame blades at 300 r/min generate larger bubbles and higher turbulent kinetic energy than propeller blades at 500 r/min. Frame blades enhance leaching efficiency by refining bubble size to improve oxygen mass transfer and by increasing turbulent kinetic energy for better mixing.

Key words: Becher process; CFD−PBM method; frame blade; reduced ilmenite; synthetic rutile; rust leaching

1 Introduction

Synthetic rutile (SR) is a titanium-rich material prepared by removing non-titanium impurities from ilmenite and is widely used in industries such as coatings, plastics, aerospace, and more [1,2]. Currently, SR is prepared using methods such as the Murso [3], Kataoka [4], Austpac [5], and Becher processes. Methods other than the Becher process often require concentrated acid leaching, which poses challenges to environmental protection. In contrast, the Becher process generates neutral wastewater, requires fewer chemical reagents, and produces recyclable pure iron oxide as a by-product, thereby reducing environmental pollution and resource wastage [6,7]. The Becher process involves the reduction of iron oxide with carbon to produce metallic iron, resulting in the formation of reduced ilmenite (RI), as shown in Reactions (1) and (2) [8]. Subsequently, the metallic iron in RI is leached out using an aerated solution, as depicted in Reactions (3)−(7) [9]:

$$2FeTiO_3+CO\rightarrow FeTi_2O_5+Fe+CO_2 \quad (1)$$

$$FeTi_2O_5+CO\rightarrow Fe+2TiO_2+CO_2 \quad (2)$$

$$Fe\rightarrow Fe^{2+}+2e \quad (3)$$

$$O_2+2H_2O+4e\rightarrow 4OH^- \quad (4)$$

$$2Fe^{2+}+5H_2O+1/2O_2\rightarrow 2Fe(OH)_3+4H^+ \quad (5)$$

$$Fe(OH)_3\rightarrow FeOOH+H_2O \quad (6)$$

$$2FeOOH\rightarrow Fe_2O_3+H_2O \quad (7)$$

Due to the significance of environmental issues, the Becher process has been increasingly applied. However, the rust leaching step in industrial settings is plagued by inefficiency, sometimes taking up to 20 h and thus becoming a major source of energy costs [10]. In light of this, researchers have proposed various strategies to enhance rust leaching efficiency [11−16]. Some

Corresponding author: Ting-an ZHANG, Tel: +86-13840205331, E-mail: zta2000@163.net;
Qiu-yue ZHAO, Tel: +86-13840142982, E-mail: zhaoqy@smm.neu.edu.cn
https://doi.org/10.1016/S1003-6326(25)66923-8

studies suggest increasing oxygen pressure to improve rust leaching efficiency, but this could result in more pronounced "in-situ rusting," which may lower the grade of synthetic rutile [11,12]. Furthermore, some researchers have explored rust leaching catalysts, including citric acid [13], acetic acid [14], organic acids, as well as sugars like sucrose [15], glucose [16], and their roles in rust leaching. These additives indeed improve efficiency, and their primary mechanism is currently believed to be the reduction of pH value. In the past decade, BRUCKARD et al [10,17] reported anthraquinone sulfonate-based redox catalysts that can enhance the rate of oxygen reduction reactions, thereby improving rust leaching rates. However, due to cost considerations, these catalysts have not yet been industrially applied. Additionally, optimizing the mixing effect of gas−liquid−solid three-phase systems is another way to improve rust leaching efficiency. Our previous research also indicated that converting traditional vertical reactors into horizontal ones is also an effective method for improving rust leaching efficiency [18].

For the rust leaching process, an ideal stirring blade should achieve the uniform suspension of solid particles and promote the dispersion of oxygen. In industries such as food and fermentation, during the rust leaching process [19], as the reaction progresses, the accumulation of iron oxides increases, leading to a rise in the solid content of the slurry. Consequently, a propeller blade may not operate efficiently under these conditions. Using impellers with combined or mixed geometries is a more effective solution. ESPINOSA et al [20] reported that a combination of Rushton turbines and helical ribbon impellers demonstrated superior mixing performance in xanthan gum solutions compared to individual impellers. KAMLA et al [21] studied the effects of the geometric shapes, number of blades, and tilt angles of anchor impellers on mixing efficiency, showing that the new impellers can significantly enhance fluid flow. Effectively improving mixing characteristics can be achieved by increasing the number of blades and tilt angles. KAZEMZADEH et al [22] reported the combination of anchor and Scaba impellers, noting that the consistency index and speed ratio of the two impellers are important factors influencing mixing efficiency. In conclusion, improving mixing effects through combinations and changes in impeller shapes can enhance process efficiency.

Currently, there are few reports on the optimization of stirring blades in the leaching field, and no numerical simulation studies have been conducted. To address this gap, in this work, a frame blade was proposed to enhance the leaching efficiency and numerical simulations were conducted to investigate its mechanism. Then, the impact of temperature, rotation speed, and additives on leaching efficiency was examined. Finally, the acceleration mechanism was discussed through kinetics analysis and CFD simulations. This study aims to pave the way for optimizing vertical rust leaching reactors by investigating the role of frame blade in rust leaching process.

2 Experimental

2.1 Materials

RI specimen utilized in this investigation was obtained from a manufacturer located in Guangxi, China. Samples with a high iron metallization efficiency were produced using a rotary kiln reduction process. The AR reagents were procured from the National Pharmaceutical Chemical Reagent Co., Ltd., China.

Table 1 shows the main chemical compositions of RI. The results reveal that RI is predominantly composed of 60.0 wt.% TiO_2 and 27.3 wt.% metallic iron (MFe), with 4.31 wt.% FeO, alongside trace amounts of Mn, Si, Mg, and Al. The iron metallization efficiency of RI is 89.4%. The structure and morphology of RI were analyzed through XRD, SEM, and particle size testing, with specific results illustrated in Fig. 1. The SEM micrograph (Fig. 1(a)) reveals the presence of irregularly embedded particles on the surface of RI. The EDS point results (Fig. 1(b)) indicate that the embedded small particles are metallic iron, and the matrix consists of TiO_2. Figure 1(c) indicates that 80% of RI particles are distributed within the range of 126−325 μm. The XRD patterns (Fig. 1(d)) elucidate that RI is primarily composed of metallic iron (MFe), rutile (TiO_2), and a minor quantity of

Table 1 Main chemical compositions of RI (wt.%)

TiO_2	MFe[a]	FeO	TFe[b]	CaO	MgO	Al_2O_3	SiO_2	Mn
60.0	27.3	4.31	30.55	0.227	0.36	1.09	1.45	1.05

[a] Metallic iron (MFe); [b] Total iron (TFe)

pseudobrookite ($FeTi_2O_5$).

2.2 Experimental equipment and method

The experiment was conducted in a 3L glass vessel, equipped with an inlet tube and a water bath. Two varieties of impellers were employed: the modified frame blade and the propeller blade commonly used in the rust leaching process. The schematic diagram of the experimental system is depicted in Fig. 2.

During the rust leaching experiment, a 1.8 L 2% (mass-to-volume ratio) NH_4Cl solution was first heated in a water bath, followed by the agitation of the solution after adding RI. Compressed air was continuously introduced into the solution through air tubes, maintaining a gas flow rate of 0.1 $m^3/(L·h)$. Solid-phase samples were extracted every 2 h and subsequently washed to remove iron oxides. Additional water was added to compensate for solution loss due to evaporation and atomization in the airflow. After the experiment, fine iron oxides were separated using a wet screening method to obtain SR. The SR was then dried and analyzed, while the iron oxides were isolated for subsequent examination.

2.3 CFD simulation

In this study, gas−liquid−solid three-phase mixing process in the rust leaching process was simulated using ANSYS Fluent software. The Euler−Euler model was employed to establish momentum equations and continuity equations for the phases, while the standard K−ε (K is the turbulent kinetic energy; ε is the turbulence energy dissipation rate) turbulence model was utilized to simulate turbulence [23]. A pseudo-transient solver was applied to solving the model's discrete equations.

During the simulation process, the multiple reference frame (MRF) method based on a steady-state algorithm was employed. The network topologies of the reactor equipped with the frame blade and the propeller blade are depicted in Figs. 3(a, b), respectively. For the MRF method, the reactor region was divided into two distinct areas: the stationary external region and the internally rotating region due to the rotation of the impeller, as depicted in Fig. 3. To enhance the result accuracy, a finer mesh was applied to the rotating internal region [24]. Additionally, the outer layer was defined as the non-rotating region using a coarser

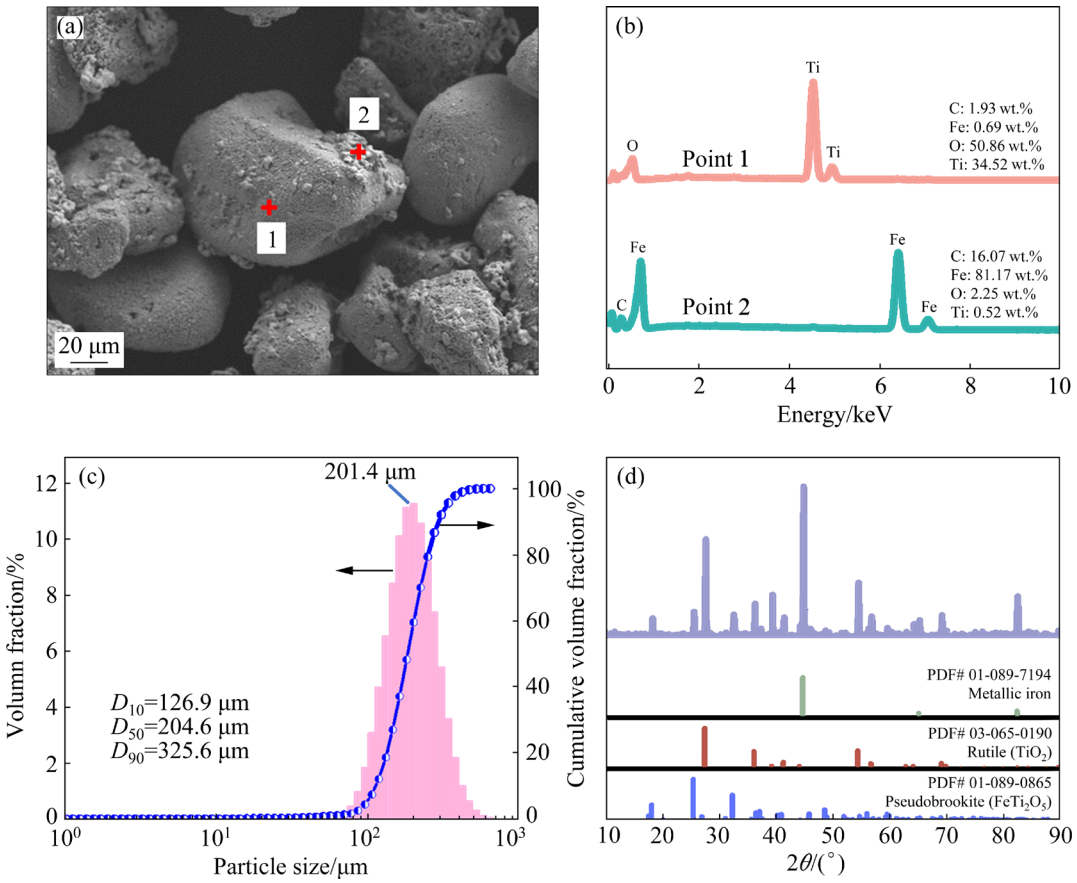

Fig. 1 SEM image (a), EDS point results (b), particle size distribution (c) and XRD patterns (d) of RI

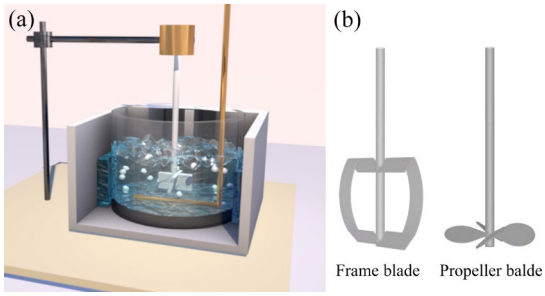

Fig. 2 Schematic diagram of experimental setup (a) and stirring blade (b)

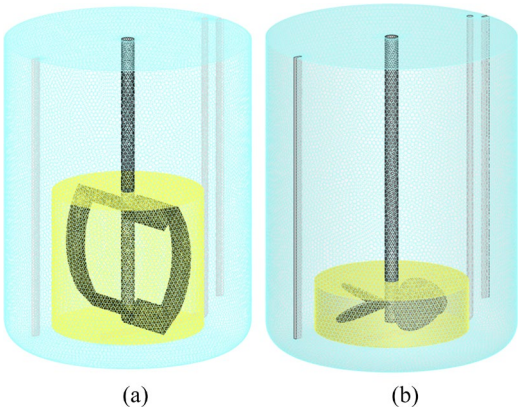

Fig. 3 Grid topologies set of reactor equipped with frame blade (a) and propeller blade (b)

mesh. For the frame blade and the propeller blade, simulations were conducted with 601773 and 427773 grids, respectively. A population balance model (PBM) was employed, with bubble size ranging from 1 to 8 mm [24−27]. The particle diameter and density of solid-phase particles are 200 μm and 4200 kg/m³, respectively, derived from TiO_2 test results. The axial filling length (H) of the reactor was 0.1 m, and the data were processed using Tecplot software.

2.4 Electrochemical methods

The electrochemical impedance spectroscopy (EIS) measurements were conducted using the Zahner electrochemical workstation (Zennium Pro, Germany). The metallic iron electrode consisted of a 10 mm × 10 mm × 5 mm metal iron block. After soldering the sample to wires, it was embedded in epoxy resin to serve as the working electrode. The exposed area was a square with a surface area of 1 cm^2, facilitating control over the corrosion area. Samples were polished with silicon carbide paper to P3000 grit, followed by ultrasonic cleaning with ethanol, rinsing with distilled water, and drying [28,29]. Platinum foil was employed as the counter electrode, and the Ag/AgCl electrode (saturated with potassium chloride) served as the reference electrode. The EIS tests were carried out in the frequency range from 100 kHz to 10 mHz, applying a sinusoidal AC perturbation with an amplitude of 10 mV (root mean square) relative to the open circuit potential [30,31]. The acquired EIS data underwent equivalent circuit fitting using ZsimpWin software. The schematic diagram of the electrochemical testing equipment is shown in Fig. S1 in the Supplementary Information.

2.5 Analytical method

The metallic iron content of the samples was determined by potassium dichromate titration [18]. The leaching efficiency (μ) was defined as follows:

$$\mu = \left(1 - \frac{w_1 m_1}{w_0 m_0}\right) \times 100\% \quad (8)$$

where w_0 is the mass fraction of metallic iron in RI, m_0 is the mass of RI, w_1 is the mass fraction of metallic iron in the samples obtained during the leaching process, and m_1 is the mass of the synthetic samples obtained during the leaching process.

The morphology and composition of the samples were characterized using a scanning electron microscopy equipped with an energy dispersive spectrometer (SEM−EDS, ZEISS Gemini 300, Germany), a particle size analyzer (Laser Particle Sizer, BT−9300S, China), an X-ray fluorescence spectrometer (XRF, ZSXPrimusIV, America), and an X-ray diffractometer (XRD, D8 Advance, Germany).

3 Results and discussion

3.1 Effect of frame paddles on rust leaching process

Three single-factor experiments were carried out on reactors equipped with both frame and propeller blades. In these experiments, temperature, stirring speed, and hydrochloric acid addition were varied, to evaluate the effect of frame blade on the metal iron removal efficiency. The temperature, hydrochloric acid concentration, and stirring speed were 50−80 °C, 1.5% (mass-to-volume ratio), and 300−500 r/min, respectively.

The results of temperature experiments are shown in Figs. 4(a, b). As the temperature increases, the corrosion rate of metallic iron correspondingly

rises [32], resulting in a continuous increase in leaching efficiency. The leaching efficiency indicator, set to measure the completion of the reaction, is established at 95%. When employing frame blades, the reaction concludes approximately after 11 h; whereas with propellers, it takes around 16 h. The application of framed blades shortens the reaction time by 5 h and significantly improves the rust leaching efficiency.

As shown in Figs. 4(c, d), the results of the stirring speed experiment indicate that leaching efficiency increases with increasing stirring speed. It is noteworthy that even under the condition of 300 r/min, the frame blades still outperform the propellers at 500 r/min in terms of leaching efficiency.

Previous research showed that the addition of hydrochloric acid can enhance leaching efficiency [14]. Therefore, we conducted experiments utilizing a 1.5% hydrochloric acid to compare these two types of blades. The experimental results, as shown in Fig. 4(e), demonstrate a significant improvement

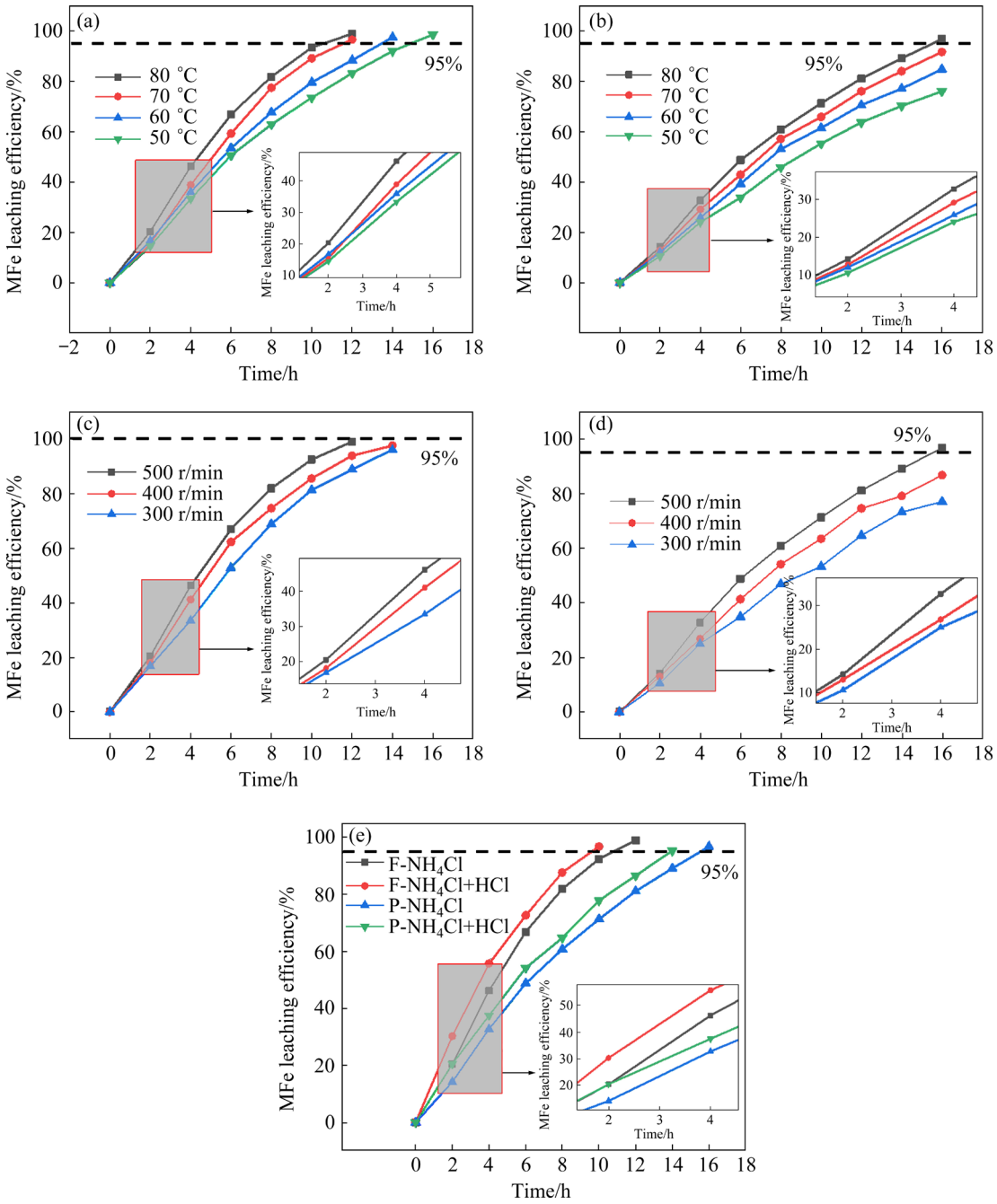

Fig. 4 Effect of temperature (a, b), stirring speed (c, d) and addition of 1.5% hydrochloric acid (e) on leaching efficiency of metallic iron from RI using frame blade (a, c, e) and propeller blade (b, d, e) (The NH_4Cl concentration was 2% in all experiments, and “F” and “P” mean frame and propeller blades, respectively)

in leaching efficiency after the addition of hydrochloric acid. The leaching time was reduced to 10 h with frame blades, and to 14 h with propellers.

We conducted SEM and XRD analyses on samples obtained after the completion of leaching. The morphology of the leached products is depicted in Figs. 5(a, b). Upon observation, the small particles protruded from the surface disappeared, leaving numerous pores on the substrate. Further magnification (Fig. 5(b)) reveals that the walls of the pores are adorned with small particles. The EDS point testing of the substrate and particles, as depicted in Fig. 5(d), indicates that the substrate is primarily TiO_2, and the small particles consist of iron oxides. This phenomenon is attributed to the "in-situ rusting" phenomenon [4,8] during the leaching process, where some leached Fe^{2+} cannot promptly enter the solution and precipitates in the pores through oxidation and hydrolysis, thus impeding the diffusion of Fe^{2+}. The XRD pattern in Fig. 5(c) shows that the product primarily consists of rutile-phase titanium dioxide, along with residue of titanium−iron oxide unreduced during the reduction step.

3.2 Kinetics results of rust leaching

The process of leaching metallic iron from rusted ilmenite is essentially a solid−liquid reaction. As depicted in the SEM images in Fig. 5, the product retains a shell. Therefore, we utilized the unreacted shrinking core model (USCM) [33,34] to compare and evaluate the leaching kinetics characteristics obtained using the two types of blades. Generally, the reaction rate is primarily determined by one of three factors: liquid film diffusion, internal diffusion within the product layer, and surface chemical reaction. The kinetic equations for these three cases are as follows:

$$r=k_1t \tag{9}$$

$$1-3(1-r)^{2/3}+2(1-r)=k_pt \tag{10}$$

$$1-(1-r)^{1/3}=k_rt \tag{11}$$

where r represents rust leaching efficiency of metallic iron; k_l, k_p and k_r are the apparent rate constants (min^{-1}) for diffusion in the liquid film layer, diffusion within the product layer, and surface chemical reaction, respectively; t is the time (min).

After fitting the experimental data obtained under different conditions using Eqs. (9)−(11), it

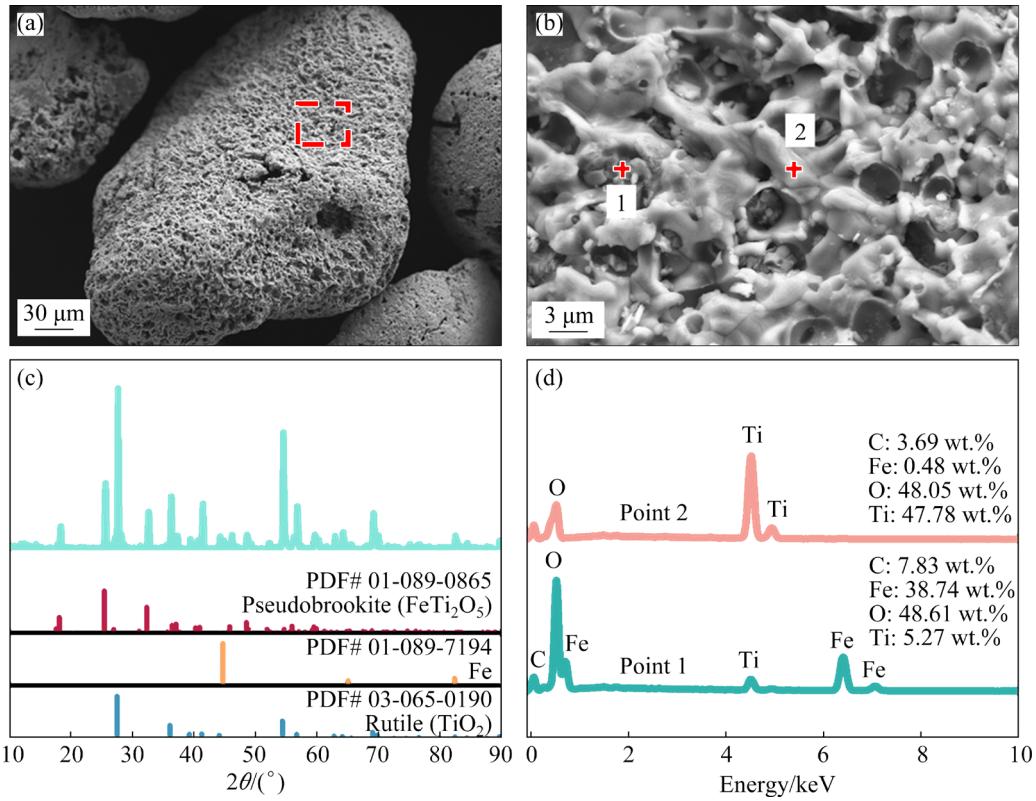

Fig. 5 SEM images with different magnifications (a, b), XRD (c), and corresponding EDS point results (d) of products obtained after rust leaching

was found that the fitting coefficient of Eq. (11) was the highest. The fitted curves are depicted in Figs. 6(a, b), while the correlation coefficients (R^2) and apparent rate constants (k) are summarized in Table 2. The results indicate that the rust leaching process is primarily controlled by surface chemical reaction, which is consistent with previous reports [16]. In particular, the apparent reaction rate constant of frame blades exceeds that of propeller blades, suggesting that frame blades enhance the reaction rate. This enhancement is likely attributable to their ability to accelerate oxygen mass transfer, thereby increasing the dissolved oxygen content and subsequently enhancing the leaching efficiency.

Table 2 Apparent rate constant k values and correlation coefficient R^2 in kinetic model of $1-(1-r)^{1/3}=kt$

Temperature/ °C	Frame blade		Propeller blade	
	$k/10^{-3}$ min^{-1}	R^2	$k/10^{-3}$ min^{-1}	R^2
50	42.23	0.98	24.21	0.99
60	48.28	0.98	29.17	0.99
70	54.83	0.99	34.66	0.99
80	60.18	0.98	40.69	0.98

To validate the rust leaching kinetics results, the electrochemical impedance spectroscopy (EIS) testing on metallic iron was conducted to analyze its electrochemical corrosion kinetics. The Nyquist plot and fitted circuit of the EIS are illustrated in Fig. 6(c) and Fig. S2 in the Supplementary Information, respectively. In the temperature range of 50−80 °C, the Nyquist plot of the electrochemical impedance spectrum at the start of the rust reaction (marked as 0 h in the curve) consists of two depressed semicircles at high frequency (HF) and low frequency (LF), both fitted with capacitor circuits, as illustrated in Fig. S2(a) in the Supplementary Information. The capacitor circuit at HF is associated with the presence of charge transfer resistances and Faradaic double layer capacitance, while the capacitor circuit at LF is formed by resistance and capacitance of adsorbed substances, such as iron ammine complexes. The appearance of the capacitor circuit representing charge transfer indicates that charge transfer is limited, and the reaction is controlled by electrochemical reaction. From 0 to 12 h, the Nyquist plot transits from two depressed semicircles in the first quadrant to one depressed semicircle at HF in the first quadrant and one at LF in the fourth quadrant. The depressed semicircle in the fourth quadrant is fitted with an inductive circuit, attributed to the large amount of iron oxides produced in the later stages of rusting. Throughout this process, no

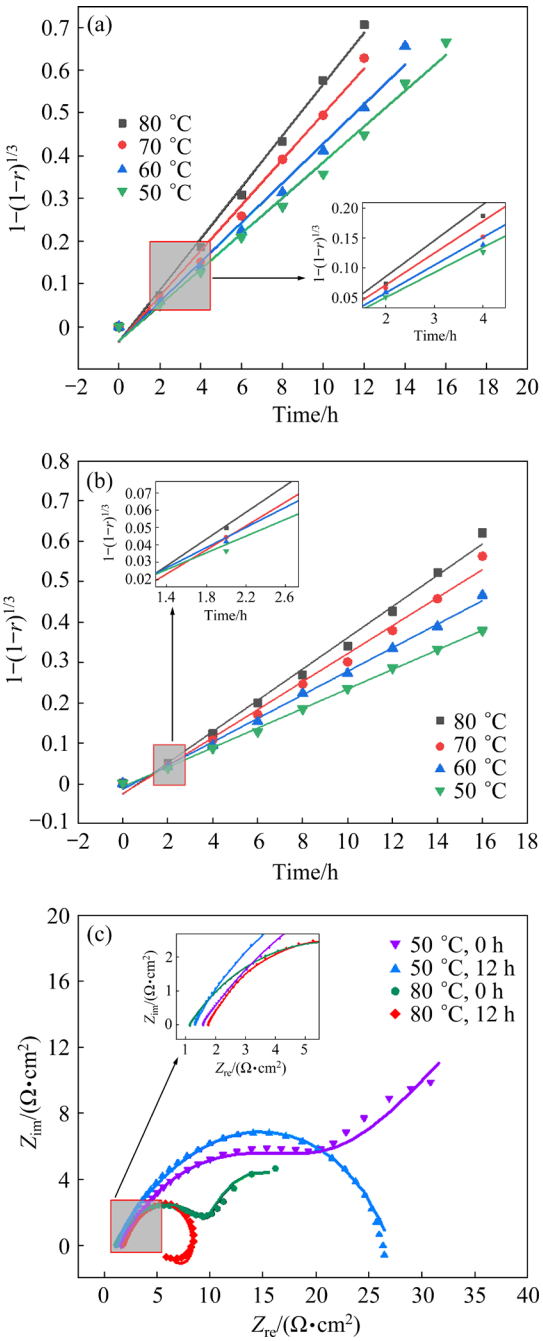

Fig. 6 (a, b) Relationship between $1-(1-r)^{1/3}$ and leaching time in temperature-variable experiments using frame blade and propeller blade, respectively; (c) EIS results of metallic iron in different rust leaching conditions (The points represent the results of EIS; The solid line represents the results fitted with the equivalent circuit in Fig. S2 in the Supplementary Information)

Warburg impedance (characterized by a straight line with a 45° slope) is observed, indicating that the rusting process belongs to the electrochemical control [35−38].

3.3 Simulation results of gas−liquid−solid three-phase mixture and mass transfer characteristics

A combined approach of computational fluid dynamics (CFD) simulation and population balance model (PBM) was employed to investigate the mixing and mass transfer performance of frame blade and propeller blade in the reactor. During the computation process, a solid loading of 10% was used, with stirring speeds ranging from 300 to 500 r/min.

Figures 7(a, b), (c, d), and (e, f) depict the flow fields generated by frame blade and propeller blade at 300, 400, and 500 r/min, respectively. The color intensity in the contour and streamlines represents the magnitude of velocity in each region. It can be observed that with the increase in the stirring speed, the velocity of the liquid in the system increases, and the flow field generated by the blade primarily develops along the axial direction. The larger stirring area of the frame blade results in higher flow velocities throughout the field, with reduced velocity attenuation.

Turbulent kinetic energy, which describes the distribution of fluid flow intensity and kinetic energy during agitation, serves as an effective indicator for evaluating mixing efficiency. Figures 8, S3 and S4 in the Supplementary Information respectively illustrate the distribution of turbulent kinetic energy under conditions of 500, 400, and 300 r/min. The axial slice at 500 r/min (Fig. 8) shows that the turbulent kinetic energy generated by frame blade far exceeds that of the propeller blade. Its is maximal near the blade and its distribution remains relatively uniform in regions farther away from the blades. In contrast, the propeller blade generates less turbulent kinetic energy, which attenuates more quickly. Similar differences are observed at 400 and 300 r/min, which also contribute to the higher leaching efficiency of the frame blades. Additionally, at 300 r/min, the frame blade still generates more turbulent kinetic energy than the propeller blade at 500 r/min, which may account for the superior leaching efficiency of the frame blade at 300 r/min compared to that of the propeller blade at 500 r/min.

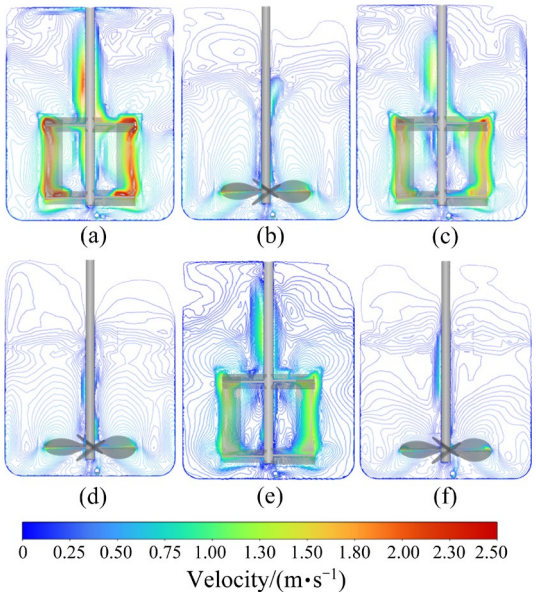

Fig. 7 Flow field and velocity magnitudes generated by frame blade (a, c, e) and propeller blade (b, d, f) at different stirring speeds: (a, b) 500 r/min; (c, d) 400 r/min; (e, f) 300 r/min

In gas−liquid−solid three-phase systems, the size distribution of bubbles plays a crucial role in the interphase mass transfer efficiency of oxygen. Smaller bubbles can enhance the mass transfer efficiency of oxygen [24]. Therefore, we evaluated the bubble size distribution under different conditions. Under the condition of 500 r/min, frame blade exhibits a significant presence of small bubbles in the 0−2.3 mm range (Fig. 9), compared to the bubble size distribution of the propeller blade (as shown in Fig. 10), which notably enhances the oxygen mass transfer efficiency. The formation of small bubbles is mainly attributed to the collision between bubbles and the stirring blades, as well as the presence of high turbulent kinetic energy [24,39]. The lower turbulent kinetic energy generated by the propeller, coupled with the limited area where the blades interact with the fluid, results in less efficient bubble breakup, allowing bubbles to grow larger as they rise. Consequently, primarily large bubbles exist during the agitation process with the propeller blade. Even with reduced stirring speeds at 400 and 300 r/min (Figs. S5 and S6 in the Supplementary Information), the frame blade still produces an abundance of small bubbles. However, the bubble size distribution of the propeller at 400 and 300 r/min (Figs. S7 and S8 in the Supplementary Information) indicates that with decrease in stirring speed, bubble growth accelerates significantly, with a noticeable increase in large bubbles (5.3−8.0 mm)

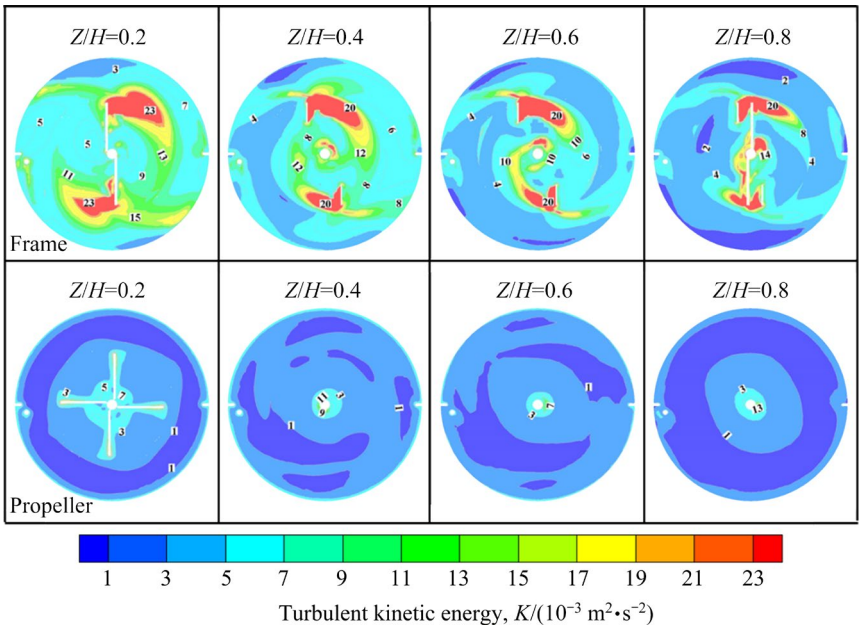

Fig. 8 Axial turbulent kinetic energy contour plots of frame blade and propeller blade at 500 r/min (Z indicates the axial length of the slice, and H represents the loading height of the reactor)

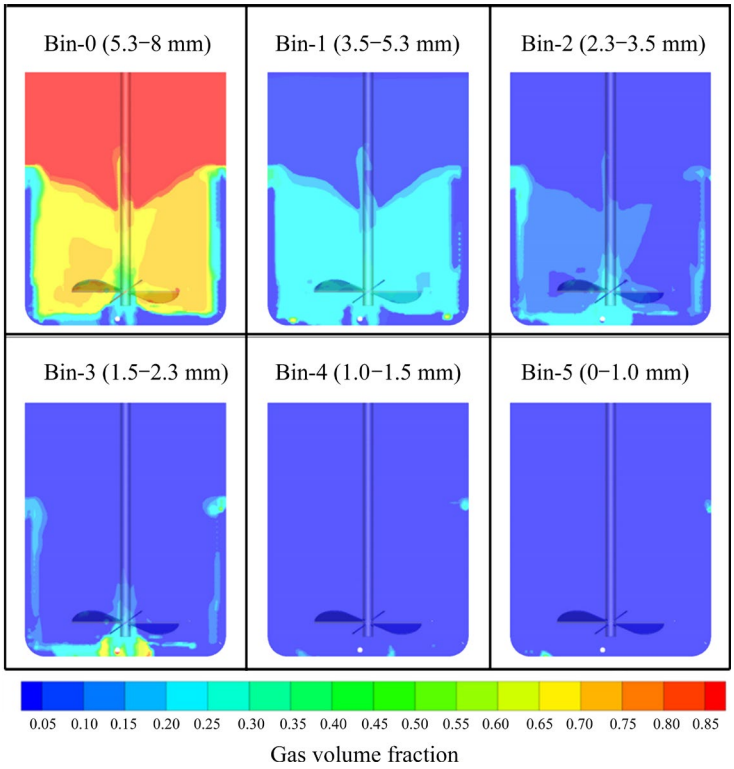

Fig. 9 Bubble size distribution generated by frame blade at 500 r/min

and a decrease in bubbles ranging from 3.5 to 5.3 mm. Therefore, the superior ability to fragment and refine bubbles is one of the reasons why frame blade can enhance the efficiency of rust leaching.

The suspension of solid particles also plays a crucial role in affecting the efficiency of rust leaching. The solid distribution of frame and propeller blades at 500 r/min is shown in Figs. 11(a) and (b), respectively. Observations show that both can suspend solid particles uniformly, indicating that solid mixing efficiency is not one of the reasons why frame blades enhance leaching efficiency.

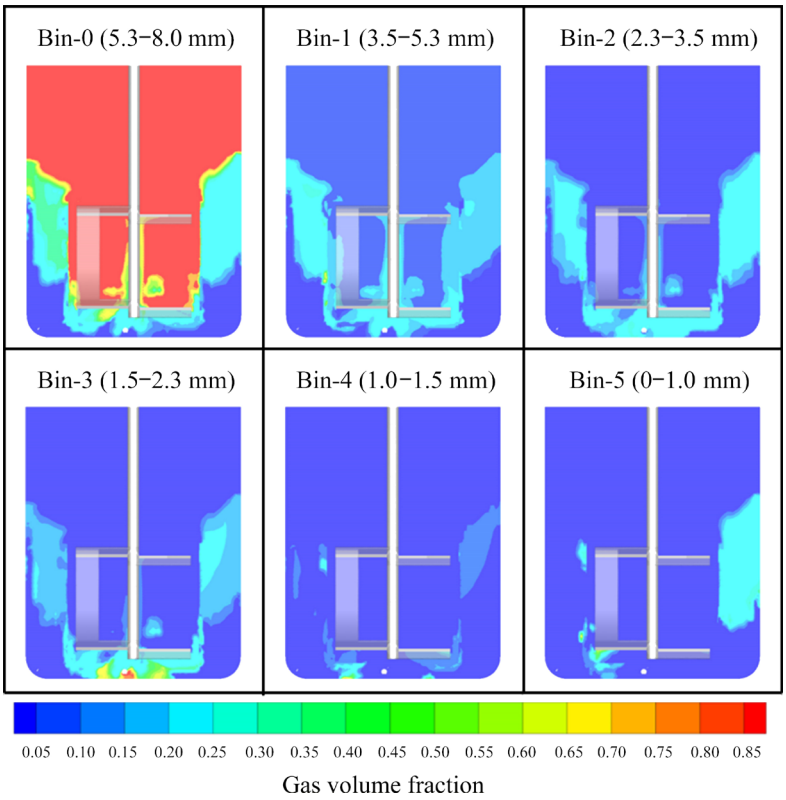

Fig. 10 Bubble size distribution generated by propeller blade at 500 r/min

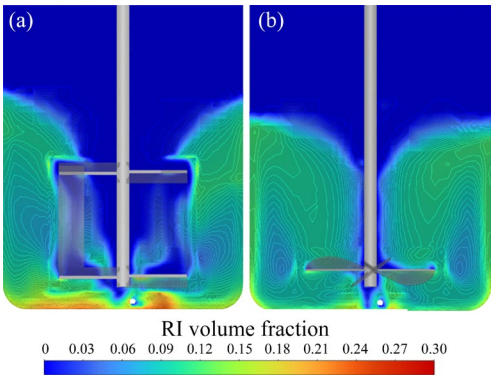

Fig. 11 Solid particle distribution generated by frame blade (a) and propeller blade (b) at 500 r/min

4 Conclusions

(1) Under the conditions of 1.5% HCl, 2% NH_4Cl, 500 r/min, and 80 °C, the reaction time is reduced from 15 h with the propeller blade to 11 h with the frame blade.

(2) Leaching process is primarily controlled by surface chemical reactions. EIS tests on metallic iron confirm that the rusting process is consistently controlled by electrochemical reactions, consistent with the kinetics results obtained from the leaching process.

(3) CFD−PBM method shows that the frame blade generates a predominantly axial flow field with higher velocities and lower attenuation. The stronger fragmentation capability of the frame blade results in a large number of small bubbles, enhancing oxygen mass transfer efficiency. This is the primary reason for the improved leaching efficiency.

CRediT authorship contribution statement

Lei ZHOU: Conceptualization, Methodology, Data curation, Writing – Original draft; **Qiu-yue ZHAO:** Resources, Supervision; **Guo-zhi LV:** Project administration, Supervision; **Zhi-he DOU:** Software, Supervision; **Ting-an ZHANG:** Funding acquisition, Supervision.

Declaration of competing interest

The authors declare that they have no known competing financial interests or personal relationships that could have appeared to influence the work reported in this paper.

Acknowledgments

This study was supported by the National Natural Science Foundation of China (No. U1908225) and the Cross-Integration and Collaborative Development Project of Northeastern University, China (No. N2225013).

The authors Thank Guangxi Ubridge New Material Technology Co., Ltd., China for providing reduced ilmenite.

Supplementary Information

Supplementary Information in this paper can be found at: http://tnmsc.csu.edu.cn/download/26-p3949-2024-0361-Supplementary_Information.pdf.

References

[1] ZHANG Wen-sheng, ZHU Zhao-wu, CHENG Chu-yong. A literature review of titanium metallurgical processes [J]. Hydrometallurgy, 2011, 108(3/4): 177−188.

[2] ZHANG Xiang-yu, LU Shu-xin, HE Dong-mei, CHAI Mao-zhou, WU Zhuang-zhuang, YAO Xiao-hong, YANG Yong-qiang. Antibacterial property of graphene quantum dots-modified TiO_2 nanorods on titanium dental implant [J]. Transactions of Nonferrous Metals Society of China, 2023, 33(8): 2395−2405.

[3] GUO Yu-feng, LIU Shui-shi, JIANG Tao, QIU Guan-zhou, CHEN Feng. A process for producing synthetic rutile from Panzhihua titanium slag [J]. Hydrometallurgy, 2014, 147: 134−141.

[4] RYOSUKE O S, KATSUTOSHI O, KOH T. Calciothermic reduction of titanium oxide and in-situ electrolysis in molten $CaCl_2$ [J]. Metallurgical and Materials Transactions B, 2003, 34: 287−295.

[5] MAHMOUD M H H, AFIFI A A I, IBRAHIM I A. Reductive leaching of ilmenite ore in hydrochloric acid for preparation of synthetic rutile [J]. Hydrometallurgy, 2004, 73(1/2): 99−109.

[6] GEETHA K S, SURENDER G D. Experimental and modelling studies on the aeration leaching process for metallic iron removal in the manufacture of synthetic rutile [J]. Hydrometallurgy, 2000, 56(1): 41−62.

[7] FARROW J B, RITCHIE I M, MANGANO P. The reaction between reduced ilmenite and oxygen in ammonium chloride solutions [J]. Hydrometallurgy, 1987, 18(1): 21−38.

[8] YU Zhi-gang, XIAO Jing-wu, LENG Hai-yan, CHOU Kuo-chih. Direct carbothermic reduction of ilmenite concentrates by adding high dosage of Na_2CO_3 in microwave field [J]. Transactions of Nonferrous Metals Society of China, 2021, 31(6): 1818−1827.

[9] GEETHA K S, SURENDER G D. Modelling of ammoniacal oxygen leaching of metallic iron in a stirred slurry reactor [J]. Hydrometallurgy, 1997, 44(1/2): 213−230.

[10] BRUCKARD W J, CALLE C, FLETCHER S, HORNE M D, SPARROW G J, URBAN A J. The application of anthraquinone redox catalysts for accelerating the aeration step in the Becher process [J]. Hydrometallurgy, 2004, 73(1/2): 111−121.

[11] WARD J, BAILEY S, AVRAAMIDES J. The use of ethylenediammonium chloride as an aeration catalyst in the removal of metallic iron from reduced ilmenite [J]. Hydrometallurgy, 1999, 53(3): 215−232.

[12] JAYASEKERA S, MARINOVICH Y, AVRAAMIDES J, BAILEY S I. Pressure leaching of reduced ilmenite: Electrochemical aspects [J]. Hydrometallurgy, 1995, 39(1/2/3): 183−199.

[13] ZHENG Fu-qiang, LIU Xia, GUO Yu-feng, WANG Shuai, CHEN Feng, YANG Ling-zhi, JIANG Tao, QIU Guan-zhou. Transformation and separation of metallic iron in reduced ilmenite during corrosion process [J]. Journal of Iron and Steel Research International, 2020, 27: 1372−1381.

[14] XIANG Jun-yi, PEI Gui-shang, LV Wei, LIU Song-li, LV Xue-wei, QIU Gui-bao. Preparation of synthetic rutile from reduced ilmenite through the aeration leaching process [J]. Chemical Engineering and Processing: Process Intensification, 2020, 147: 107774.

[15] GUO Yu-feng, LIU Shui-shi, MA Xiao-wen, JIANG Tao, QIU Guan-zhou. Rusting kinetics of metallic iron in reduced ilmenite strengthened by hydrochloride [J]. The Chinese Journal of Nonferrous Metals, 2010, 20(10): 2038−2044. (in Chinese)

[16] KUMARI E J, BHAT K H, SASIBHUSHANAN S, MONAN DAS P N. Catalytic removal of iron from reduced ilmenite [J]. Minerals Engineering, 2001, 14(3): 365−368.

[17] FLETCHER S, BRUCKARD W J, CALLE C, CONSTANTI-CAREY K, HORNE M D, RUZBACKY R, SPARROW G J. Soluble catalysts for the oxygen reduction reaction (orr), and their application to Becher aeration [J]. Industrial & Engineering Chemistry Research, 2019, 58(24): 10190−10198.

[18] ZHOU Lei, ZHAO Qiu-yue, LV Guo-zhi, LI Mao-yuan, ZHENG Ming-zhao, ZHANG Ting-an. The application of a novel horizontal frame paddle reactor to remove metallic iron from reduced ilmenite in the Becher process [J]. Hydrometallurgy, 2022, 208: 105804.

[19] ESPINOSA T, FUENTE E, TECANTE A, TANGUY P A. Power consumption of a dual turbine–helical ribbon impeller mixer in ungassed conditions [J]. Chemical Engineering Journal, 1997, 67(3): 215−219.

[20] ESPINOSA T, FUENTE E, TECANTE A, MEDINA-TORRES L, TANGUY P A. Mixing time in rheologically evolving model fluids by hybrid dual mixing systems [J]. Chemical Engineering Research and Design, 2002, 80: 817−823.

[21] KAMLA Y, AMEUR H, KARAS A, ARAB M I. Performance of new designed anchor impellers in stirred tanks [J]. Chemical Papers, 2020, 74: 779−785.

[22] KAZEMZADEH A, EIN-MOZAFFARI F, LOHI A, PAKZAD L. Effect of the rheological properties on the mixing of Herschel−Bulkley fluids with coaxial mixers: Applications of tomography, CFD, and response surface methodology [J]. The Canadian Journal of Chemical Engineering, 2016, 94(12): 2394−2406.

[23] ZHU Shuai, ZHAO Qiu-yue, LI Xiao-long, LIU Yan, ZHANG Ting-an. CFD simulation of gas-slag-metal multiphase flow in a side-blown vortex smelting reduction reactor [J]. Journal of Sustainable Metallurgy, 2023, 9: 1033−1049.

[24] AMIRAFTABI M, KHIADANI M, MOHAMMED H A, ARSHAD A. CFD-PBM and experimental investigation of a shear thinning fluid in a gas−liquid tank agitated by a helical ribbon impeller [J]. Separation and Purification Technology, 2021, 272: 118855.

[25] YANG Shi-fang, LI Xiang-yang, YANG Chao, MA Bin, MAO Zai-sha. Computational fluid dynamics simulation and experimental measurement of gas and solid holdup distributions in a gas–liquid–solid stirred reactor [J]. Industrial & Engineering Chemistry Research, 2016, 55(12): 3276−3286.
[26] ZHANG Yan-hong, BAI Yu-lan, WANG Hua-lin. CFD analysis of inter-phase forces in a bubble stirred vessel [J]. Chemical Engineering Research and Design, 2013, 91(1): 29−35.
[27] MALUTA F, ALBERINI F, PAGLIANTI A, MONTANTE G. Hydrodynamics, power consumption and bubble size distribution in gas−liquid stirred tanks [J]. Chemical Engineering Research and Design, 2023, 194: 582−596.
[28] CHEN Wen-jing, YE Nan, ZHUO Hai-ou, TANG Jian-cheng. Electrochemical corrosion behaviour of Zn−Sn−Cu−*x*Ni lead-free solder alloys [J]. Transactions of Nonferrous Metals Society of China, 2023, 33(9): 2740−2750.
[29] LI Yu-feng, WANG Bo-wen, SUN Xiao-hao, LIU De-hao. Effect of MgF_2 coating on stress corrosion cracking behavior of Mg−Zn−Ca alloy in simulated body fluid [J]. Transactions of Nonferrous Metals Society of China, 2023, 33(7): 2044−2053.
[30] QIU Wei, LI Ya-wen, HUANG Gang, CHEN Jian, REN Yan-jie, HUANG Wei-ying, CHEN Wei, WU Tang-qing, YAO Mao-hai, XIONG Ai-hu. Corrosion behavior of as-cast AZ91 magnesium alloy with VN particle additions in NaCl solution [J]. Transactions of Nonferrous Metals Society of China, 2023, 33(5): 1398−1410.
[31] SILVA R M P, SUFFREDINI H B, BASTOS I N, SANTOS L F, SIMÕES A M P. Naphthenic acid corrosion of API 5L X70 steel in aqueous/oil environment using electrochemical surface-resolved and analytical techniques [J]. Electrochimica Acta, 2022, 407: 139900.
[32] ZHOU Lei, ZHAO Qiu-yue, LV Guo-zhi, DOU Zhi-he, MU Wang-zhong, ZHANG Ting-an. Effect of NH_4Cl on the rusting leaching behavior of metallic phase of iron in reduced ilmenite during TiO_2 purification: An electrochemical and density-functional theory study [J]. Applied Surface Science, 2023, 638: 158019.
[33] TANAYDIN M K, TANAYDIN Z B, DEMIRKIRAN N. Optimization of process parameters and kinetic modelling for leaching of copper from oxidized copper ore in nitric acid solutions [J]. Transactions of Nonferrous Metals Society of China, 2022, 32(4): 1301−1313.
[34] GUI Qi-hao, KHAN M, WANG Shi-xing, ZHANG Li-bo. The ultrasound leaching kinetics of gold in the thiosulfate leaching process catalysed by cobalt ammonia [J]. Hydrometallurgy, 2020, 196: 105426.
[35] FARSAK M, KELEŞ H, KELEŞ M. A new corrosion inhibitor for protection of low carbon steel in HCl solution [J]. Corrosion Science, 2015, 98: 223−232.
[36] SOLMAZ R. Investigation of the inhibition effect of 5-((E)-4-phenylbuta-1,3-dienylideneamino)-1,3,4-thiadiazole-2-thiol Schiff base on mild steel corrosion in hydrochloric acid [J]. Corrosion Science, 2010, 52(10): 3321−3330.
[37] LIANG Zhi-peng, JIANG Kai-xi, ZHANG Ting-an. Corrosion behaviour of lead bronze from the Western Zhou Dynasty in an archaeological-soil medium [J]. Corrosion Science, 2021, 191: 109721.
[38] FARELAS F, GALICIA M, BROWN B, NESIC S, CASTANEDA H. Evolution of dissolution processes at the interface of carbon steel corroding in a CO_2 environment studied by EIS [J]. Corrosion Science, 2010, 52(2): 509−517.
[39] WU Yong-jun, WANG Jian, YOU Pan, LUO Pei-cheng. Gas phase hydrodynamics in a surface-aerated tank with a long-short blades agitator [J]. AIChE Journal, 2023, 69(1): e17680.

框式桨叶对锈蚀浸出的强化及其机理

周 雷，赵秋月，吕国志，豆志河，张廷安

东北大学 冶金学院 特殊冶金与过程工程研究所 多金属共生矿生态化利用教育部重点实验室，沈阳 110819

摘 要：采用框式桨叶替代传统螺旋桨叶，以增强 Becher 工艺浸出步骤的效率。采用浸出实验、电化学实验和数值模拟相结合的方法。结果表明，与螺旋桨叶相比，框式桨叶显著提高了浸出效率，将反应时间从 15 h 缩短到 10 h。即使在搅拌速率为 300 r/min 时，框式桨叶的性能也优于 500 r/min 的螺旋桨叶的性能。动力学分析表明，浸出过程由表面化学反应控制。CFD−PBM 模拟显示，与 500 r/min 时的螺旋桨叶相比，300 r/min 时框式桨叶产生的气泡较大、湍流动能较高。框式桨叶通过减小气泡尺寸提高氧气传质和通过增强湍流动能实现更好的混合来提高浸出效率。

关键词：Becher 工艺；CFD−PBM 法；框式桨叶；还原钛铁矿；合成金红石；锈蚀浸出

(Edited by Wei-ping CHEN)